ACES Asian Chemical Editorial Society

DOI: 10.1002/asia.201900418

CHEMISTRY AN ASIAN JOURNAL Communication

SPECIAL ISSUE

Oxygen Microbubble Generator Enabled by Tunable Catalytic Microtubes

Sumayyah Naeem,[a, b] Farah Naeem,[a, b] Jinrun Liu,[a] Vladimir A. Bolaños Quiñones,[a] Jing Zhang,*[c] Le He,[d] Gaoshan Huang,[a] Alexander A. Solovev,*[a] and Yongfeng Mei[a]

Abstract: Rolled-up catalytic Ti/Cr/Pt microtubes, consisting of inorganic nanomembranes integrated on-chip, are used to generate oxygen microbubbles in solutions of hydrogen peroxide. Oxygen bubble parameters (frequency, radius and volumetric flow rate) are optimized at different concentrations of hydrogen peroxide and common dish soap. Increasing the aspect ratio of the microtube (e.g., tube length/diameter) leads to the formation of smaller bubbles, but at higher frequencies. Longer tubes produce less total oxygen volume in comparison to shorter tubes. We attribute this observation to the specific dynamic behaviours of bubbles in tubes.

A portable generator that liberates oxygen from liquids via chemical reactions has a number of important potential uses, including in emergency situations. In the presence of a catalyst, a significant amount of O_2 can be released by the catalytic decomposition of hydrogen peroxide ($2H_2O_2 \rightarrow 2H_2O + O_2$).[1] Despite previous designs of various oxygen generators, a better understanding of gas formation at the level of individual nano- and microparticles remains a challenge. Previously, generation of oxygen was successfully demonstrated from H_2O_2 using dry yeast.[2] García and co-workers described the oxygen generation through photocatalytic water splitting under visible light irradiation, where Zn/Cr(LDH) material was used.[3] Microporous surface of Zeolite adsorbents can separate oxygen from nitrogen contained in the ambient air.[4] Recently engineered autonomous catalytic micromotors and micropumps are capable of converting chemical energy into the kinetic energy of motion.[5–11] Mechanisms of nano/-microparticle motion include self-generated forces such as self-electrophoresis, self-diffusiophoresis and microbubble recoil.[12,13] Such micromotors are particularly attractive for environmental applications.[14,15] Other materials, such as recently demonstrated PPyNP-based micromotors powered by light can be potentially useful for delivery of biomedical cargo.[16] Other than that, when integrated on a substrate, catalytic microparticles operate as on-chip micropumps.[17] In comparison to previously existing artificial micromotors, catalytic microtubes[18–20] utilize an efficient bubble-driven pumping mechanism,[21] which helps to achieve ultrafast motion.[22,23] Light-driven Janus micromotor can move at a speed of 16 $\mu m\,s^{-1}$ under 40 $mW\,cm^{-2}$ UV light due to diffusiophoretic effects in pure water and release oxygen.[24] Formation of bubbles on the catalytic surface depends on the catalytic activities of the surface and an existence of gas-filled cavities on the surfaces.[25] Generally, gaseous oxygen molecules can reach the opposite walls and fill the microtube much faster (on the order of 10^{-3} s), in comparison to cm-scale reactors.[26] It is known that bubble nucleation requires a high concentration of gas molecules and that, typically, a heterogeneous nucleation on surfaces significantly decreases the energy barrier required for nucleation, growth and stable generation of bubbles.[27] Similar studies have reported how microtubes can enhance the generation of hydrogen[28] and release carbon dioxide gas in aqueous solutions.[11] The influence of surfactants on the formation of bubbles and on the motion of motors has been recently investigated.[29,30]

In this study, we report on the generation of oxygen microbubbles by catalytic Ti/Cr/Pt microtubes located in different concentrations of hydrogen peroxide and surfactants (common soap). The synthesis of rolled-up Ti/Cr/Pt catalytic microtubes is described in supporting information. Microtubes with different lengths, from 20 to 120 μm, are tested in aqueous H_2O_2 solutions with the addition of commercially available Walch dish soap. The influences of tubular length, concentrations of soap and peroxide fuel on the production of oxygen are examined. Here, we describe a new, portable and a facile oxygen generator using tunable catalytic microtubes. Bubbles' generation is controlled using concentrations of H_2O_2, surfactants and an aspect ratio of tubes to optimize the production of oxygen.

[a] S. Naeem, F. Naeem, J. Liu, Dr. V. A. B. Quiñones, Prof. Dr. G. Huang, Prof. Dr. A. A. Solovev, Prof. Dr. Y. Mei
Department of Materials Science
Fudan University
220 Handan Road, Shanghai 200433 (People's Republic of China)
E-mail: solovevlab@gmail.com

[b] S. Naeem, F. Naeem
State Key Laboratory for Modification of Chemical Fibers and Polymer Material Science and Engineering
Donghua University
Shanghai 201620 (People's Republic of China)

[c] Prof. J. Zhang
College of Science
Donghua University
Shanghai 201620 (People's Republic of China)
E-mail: jingzh@dhu.edu.cn

[d] Prof. L. He
Institute of Functional Nano & Soft Materials (FUNSOM)
Jiangsu Key Laboratory for Carbon-Based Functional Materials & Devices
Soochow University
199 Ren'ai Road, Suzhou, 215123, Jiangsu (People's Republic of China)

Supporting information and the ORCID identification number(s) for the author(s) of this article can be found under: https://doi.org/10.1002/asia.201900418.

This manuscript is part of a special issue on Smart Chemistry, Smart Motors. Click here to see the Table of Contents of the special issue.

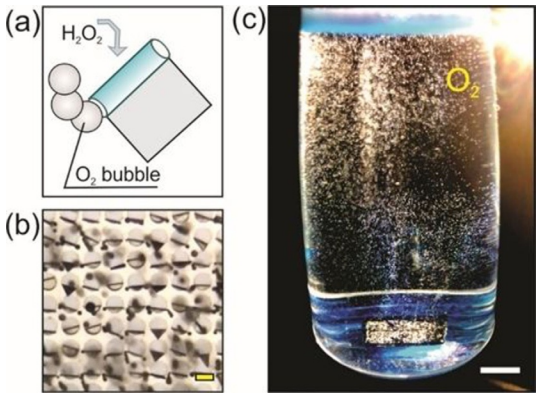

Figure 1. a) Schematic image of an individual microtube generating bubbles. b) Optical microscopy images of on-chip integrated catalytic Ti/Cr/Pt microtubes immersed in hydrogen peroxide solution. At different concentrations of peroxide fuel, the microtube generates O_2 bubbles with variable diameters, frequencies and volumetric rates. The scale bar is 20 μm. c) Optical camera image of a silicon sample with rolled-up microtubes located at the bottom of a glass containing aqueous hydrogen peroxide (12% v/v) with added surfactants (32% v/v). Visible O_2 microbubbles are generated and slowly rise in the solution. The scale bar is 1.4 cm.

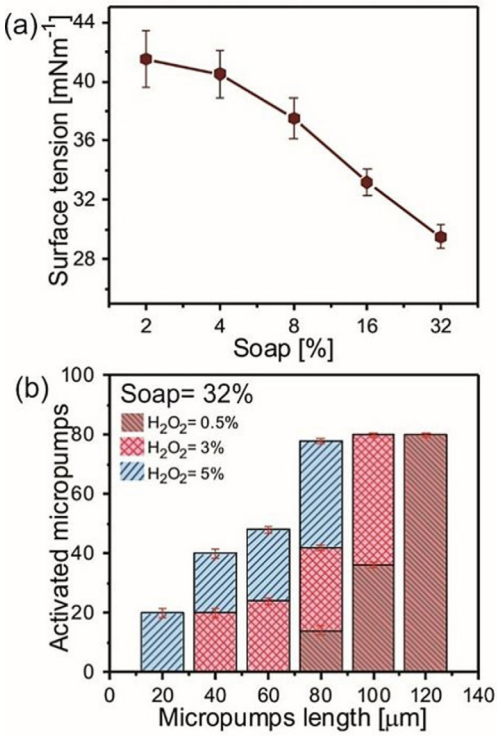

Figure 2. a) Measurement of the surface tension of solutions with different concentrations of Walch brand soap (2–32% v/v). b) Populations of activated microtubes with constant soap (32% v/v) and different H_2O_2 concentrations: 0.5% v/v (left-tilted hatched region), 3% v/v (crosshatched region) and 5% v/v (right-tilted hatched region).

Figure 1a shows a schematic image of an individual microtube, prepared by the rolled-up nanomembrane method.[18] When immersed in solutions containing H_2O_2 the microtube decomposes hydrogen peroxide and generates O_2 bubbles. Figure 1b provides an optical microscopy image of an array of catalytic microtubes producing multiple O_2 bubbles. Figure 1c shows a sample (length 1.5 cm) with on-chip integrated catalytic microtubes in the hydrogen peroxide solution. Bubbles with a diameter in the range of 20–100 μm are generated and accumulate in the solution due to their low buoyancy. Figure 2a shows the surface tension measurement of an aqueous Walch brand soap solution, measured using the maximum bubble pressure method. As expected, the surface tension of the water decreases when more soap is added. Figure 2b represents the statistical data of active tubes (length from 20 to 120 μm) in 0.5, 3 and 5% v/v H_2O_2 solutions, respectively. The activation of such microtubes in the peroxide fuel with added soap corresponds favorably to the previous report.[18] The highlighted area of the graph shows the population of activated microtubes in specific concentrations of H_2O_2: 0.5% v/v in the left-tilted hatched region; 3% v/v H_2O_2 in the crosshatched region; and 5% v/v H_2O_2 in the right-tilted hatched region. Longer tubes are activated at lower concentrations of hydrogen peroxide due to their better accumulation of molecular oxygen in reaction-diffusion processes. Longer tubes have larger coated Pt catalytic surface area in comparison to shorter tubes. Moreover, surface cavities reduce energy barrier in heterogeneous nucleation of bubbles.[27]

Surfactants play an important role in the stabilization of the air-liquid interface, decreasing the surface tension, decreasing the bubble size and increasing the bubble frequency in catalytic microtubes.[29] Figure 3a–c illustrates the dependence of the gas/bubble generation rate on the concentrations of soap for Ti/Cr/Pt tubes with different lengths (60, 80 and 100 μm) with a constant concentration of H_2O_2 (12% v/v). The maximum gas generation rate (counted by bubbles) is produced with 2% soap for 60 μm long tubes (3.1 nl hour^{-1}), in comparison to 80 μm (2.6 nl hour^{-1}) and 100 μm (2.3 nl hour^{-1}). The shorter tubes of 60 μm (5.94 Hz) produced a lower bubble frequency than the tubes of 80 μm (8.14 Hz) and 100 μm (10 Hz). Previously, a theoretical model describing mass transport in catalytic microtubes has shown that longer tubes produce more O_2 due to their higher catalytic area.[31] Contrary to this observation, however, here we experimentally observe that longer tubes produce less total O_2 volume. At the same time, higher concentrations of soap increase the frequency of bubbles and decrease the total volumetric oxygen rate.

Figure 4a illustrates the dependence of tubular length on gas generation rates and bubble radiuses at constant soap and peroxide concentrations. Shorter 20-μm-long tubes produce larger volumes of O_2 (average O_2 radius 8.9 μm, O_2 volume 12.2 nl hour^{-1}) in comparison to longer 120-μm tubes (O_2 radius 4.6 μm, O_2 volume 2.5 nl hour^{-1}) in 6% v/v H_2O_2 and 32% v/v soap solutions. When H_2O_2 is added into the solution, bubble starts to generate from the nucleation sites inside the micropump, as shown in the Figure 4e. An aspect ratio of tubes and the curvature of catalytic surface plays an important role for efficient nucleation/generation of bubbles. This creates the saturation of bubbles inside the micropumps and leads to a significant decrease in the detaching size (diameter) of microbubbles.[32] Generally, heterogeneous bubble nucleation on solid catalytic surface requires an accumulation of O_2 mole-

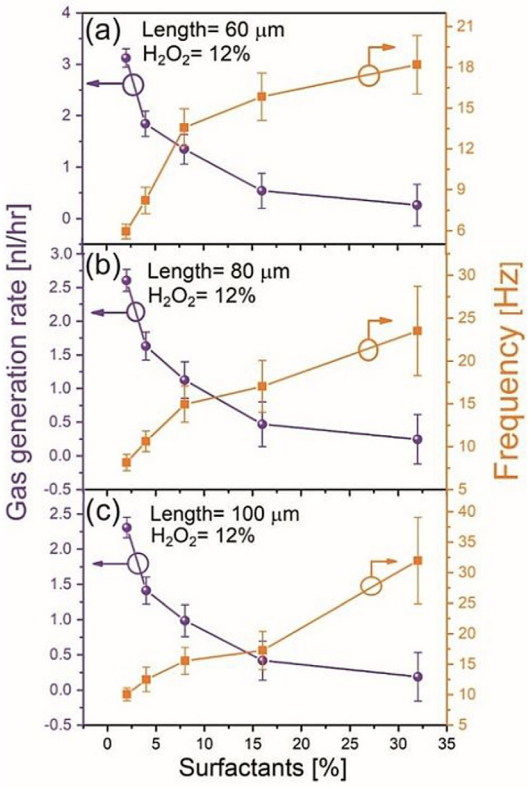

Figure 3. a–c) Analyses of gas generation rates (left *y*-axis) and bubble frequency (right *y*-axis) from different tube lengths: 60, 80 and 100 μm. Ti/Cr/Pt tubes located at a constant 12% v/v H_2O_2 solution and with different soap concentrations. An increase of soap concentration leads to an increase in bubble frequency and to a simultaneous decrease in O_2 generated volume.

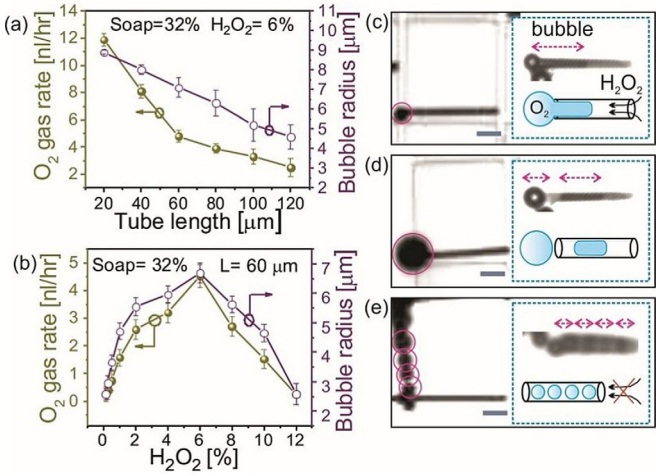

Figure 4. a) Dependence of gas generation rate on bubble radius for different tube lengths at constant concentrations of hydrogen peroxide (6% v/v) and soap (32% v/v). b) Influence of H_2O_2 concentration on the gas generation rate and the bubble radius of 60-μm-long tubes at a fixed concentration of soap (32% v/v). c) Optical micrograph of an individual microtube generating a small diameter bubble at low frequency in a low concentration of hydrogen peroxide. An inset image shows another microtube with semi-transparent walls, where the growing bubble is connected by the neck to the middle of the tube. d) Optical micrograph of the microtube generating larger diameter bubbles at a higher concentration of peroxide. An inset shows another semi-transparent tube, where the bubble is ejected and the bubble slug is located in the tube. e) Optical micrograph of the microtube generating smaller diameter bubbles in a higher concentration of peroxide fuel. An inset image shows the nucleation of multiple bubbles, which fill the tube. The scale bar is 30 μm.

cules to reach a critical nucleation energy that depends on saturation concentration of O_2 and curvature of the surface. The formation of bubbles on a concave surface requires less energy than on flat and a convex surfaces.[33] Similar, tubular structures help to reduce the energy barrier for bubble nucleation, both due to curvature and length, that is, tube aspect ratio.

Figure 4b shows the dependence of gas generation rates on the concentration of H_2O_2 and an average bubble radius for a 60-μm-long tube (values for 80 and 100 μm long tubes are not shown in the graph). At 0.125% v/v H_2O_2, the oxygen generation rates from 60-, 80- and100-μm-long tubes are 0.261, 0.24 and 0.21 nl hour^{-1}, with frequencies of 3.6, 4.1 and 4.9 Hz, respectively. At 12% v/v of H_2O_2, oxygen generation rates are 0.258, 0.245 and 0.188 nl hour^{-1} with frequencies 18.2, 23.5 and 31.98 Hz, respectively. For 60, 80 and 100 μm long tubes the maximum oxygen generation rates are 4.5 nl hour^{-1} (H_2O_2 6% v/v), 4.1 nl hour^{-1} (H_2O_2 5% v/v) and 3.8 nl hour^{-1} (H_2O_2 4% v/v), which correspond to bubble frequencies of 13.4, 16.1 and 17.8 Hz, respectively. Figure 4c–e shows an individual Ti/Cr/Pt microtube immersed in different concentrations of hydrogen peroxide 1, 4 and 10% v/v, respectively. Initially, upon an increase in the hydrogen peroxide concentration, the ejected O_2 bubble diameter increases. An inset of Figure 4c shows a semi-transparent individual tube and schematic with a growing bubble connected by the neck to the middle of the tube (t = 0). An inset of Figure 4d indicates the next moment (t = 100 ms): one bubble is ejected and the rest of the gas pocket remains in the tube. When more peroxide fuel is added, bubbles are generated at a higher frequency. An inset of Figure 4e shows a semi-transparent tube containing multiple nucleated bubbles. At lower peroxide fuel concentrations, the bubble slug continuously remains in the tube (Figure 4c,d).

Multiple bubbles at higher concentrations of fuel are continuously ejected and the nucleation of new bubbles costs more energy (Figure 4e).[34] It was previously observed that smaller bubbles migrate through the tubes and induce hydrodynamic fluid pumping.[21] In flow-focusing microfluidic devices, the volume of the generated bubbles scales as $V_b \sim \Delta p/\mu Q$, where Δp is the pressure across the dispersed phase that formed the bubble, μ is fluid viscosity and Q is the rate of fluid flow. In other words, an increase of the flow rate leads to a generation of smaller bubbles. However, in our case of catalytic microtubes, the parameters of flow rate and bubble pressure are local, and a more detailed explanation would require further investigations.

In summary, we have demonstrated an oxygen generator based on catalytic Ti/Cr/Pt microtubes with tunable lengths in the range of 20–120 μm. Longer tubes generate O_2 bubbles of smaller size at higher frequencies in comparison to shorter tubes (with all tubes containing constant surfactant and H_2O_2 concentrations). Similarly, the O_2 volumetric rate decreases with lower surface tension (at constant tube length and H_2O_2

concentration). At lower H_2O_2 concentrations, bubbles are connected by the neck to the bubble slug that remains in the tube. Such bubbles connected by the neck grow to larger diameters and volumes. At higher H_2O_2 concentrations, multiple bubbles nucleate in the tubes. Next, it will be of high interest to study how different surfactants influence the generation of oxygen bubbles.[35] An immersion of tubes in the hydrogen peroxide fuel leads to a continuous generation of oxygen bubbles at the rate of approximately 10 nl hour^{-1} per tube. We estimate that for a prototype O_2 generator, around one billion of catalytic tubes would be required to release enough oxygen (at 6% H_2O_2) and to support the O_2 needs of an individual human.

Acknowledgements

AAS is very grateful for the financial support from the young "1000 talent" plan, P. R. China. The authors also acknowledge financial support from the Natural Science Foundation of China (Grant No. 51475093), (Grant No. 51850410502).

Conflict of interest

The authors declare no conflict of interest.

Keywords: bubbles · catalyst · hydrogen peroxide · microtubes · oxygen

[1] L. W. Hall, R. E. Kellagher, K. J. Fleet, *Anaesthesia* **1986**, *41*, 516 – 518.
[2] J. H. Burness, *J. Chem. Educ.* **1996**, *73*, 851.
[3] C. G. Silva, Y. Bouizi, V. Fornés, H. Garcı, *J. Am. Chem. Soc.* **2009**, *131*, 13833 – 13839.
[4] M. Pan, H. M. Omar, S. Rohani, *Nanomater.* **2017**, *7*, 195.
[5] W. F. Paxton, P. T. Baker, T. R. Kline, Y. Wang, T. E. Mallouk, A. Sen, *J. Am. Chem. Soc.* **2006**, *128*, 14881 – 14888.
[6] P. Fischer, M. Pumera, J. Wang, *Adv. Funct. Mater.* **2018**, *28*, 1801745.
[7] J. G. Gibbs, Y.-P. Zhao, *Small* **2009**, *5*, 2304 – 2308.
[8] K. K. Dey, A. Sen, *J. Am. Chem. Soc.* **2017**, *139*, 7666 – 7676.
[9] H. Zhu, S. Nawar, J. G. Werner, J. Liu, G. S. Huang, Y. F. Mei, D. A. Weitz, A. A. Solovev, *J. Phys. Condens. Matter* **2019**, *31*, 214004 – 214012.
[10] J. R. Howse, R. A. L. Jones, A. J. Ryan, T. Gough, R. Vafabakhsh, R. Golestanian, *Phys. Rev. Lett.* **2007**, *99*, 048102 – 048105.
[11] Y. Zhang, H. Zhu, W. Qiu, Y. Zhou, G. S. Huang, Y. F. Mei, A. A. Solovev, *Chem. Commun.* **2018**, *54*, 5692 – 5695.
[12] H. P. Ning, Y. Zhang, H. Zhu, A. Ingham, G. S. Huang, Y. F. Mei, A. A. Solovev, *Micromachines* **2018**, *9*, 75 – 110.
[13] L. Liu, T. Bai, Q. Chi, Z. Wang, S. Xu, Q. Liu, Q. Wang, *Micromachines* **2017**, *8*, 267 – 283.
[14] L. Soler, S. Sanchez, *Nanoscale* **2014**, *6*, 7175 – 7182.
[15] W. Gao, J. Wang, *ACS Nano* **2014**, *8*, 3170 – 3180.
[16] Y. Sun, Y. Liu, B. Song, H. Zhang, R. Duan, D. Zhang, B. Dong, *Adv. Mater. Interfaces* **2019**, *6*, 1801965 – 1801971.
[17] M. E. Ibele, Y. Wang, T. R. Kline, T. E. Mallouk, A. Sen, *J. Am. Chem. Soc.* **2007**, *129*, 7762 – 7763.
[18] A. A. Solovev, Y. F. Mei, E. Bermudez Urena, G. S. Huang, O. G. Schmidt, *Small* **2009**, *5*, 1688 – 1698.
[19] W. Xi, A. A. Solovev, A. N. Ananth, D. H. Gracias, S. Sanchez, O. G. Schmidt, *Nanoscale* **2013**, *5*, 1294 – 1297.
[20] A. Klingner, I. S. M. Khalil, V. Magdanz, V. M. Fomins, O. G. Schmidt, S. Misra, *J. Phys. Chem. C* **2017**, *121*, 14854 – 14863.
[21] A. A. Solovev, S. Sanchez, Y. F. Mei, O. G. Schmidt, *Phys. Chem. Chem. Phys.* **2011**, *13*, 10131 – 10135.
[22] S. Sanchez, A. A. Solovev, Y. Mei, O. G. Schmidt, *J. Am. Chem. Soc.* **2010**, *132*, 13144 – 13145.
[23] S. Sanchez, A. N. Ananth, V. M. Fomin, M. Viehrig, O. G. Schmidt, *J. Am. Chem. Soc.* **2011**, *133*, 14860 – 14863.
[24] Q. Zhang, R. Dong, Y. Wu, W. Gao, Z. He, B. Ren, *ACS Appl. Mater. Interfaces* **2017**, *9*, 4674 – 4683.
[25] F. Yang, M. Manjare, Y. Zhao, R. Qiao, *Microfluid. Nanofluid.* **2017**, *21*, 6 – 17.
[26] B. Rogers, S. Pennathur, J. Adams in Nanotechnology Understanding Small System, 2nd Edition, CRC Press, Boca Raton, **2011**, pp. 284 – 322.
[27] S. F. Jones, G. M. Evans, K. P. Galvin, *Adv. Colloid Interface Sci.* **1999**, *80*, 27 – 50.
[28] R. V. Franca, A. Thursfield, I. S. Metcalfe, *J. Membr. Sci.* **2012**, *389*, 173 – 181.
[29] S. Naeem, F. Naeem, M. Manjare, F. Liao, V. A. Bolanos Quinones, G. S. Huang, Y. Li, J. Zhang, A. A. Solovev, Y. F. Mei, *Appl. Phys. Lett.* **2019**, *114*, 033701.
[30] H. Wang, G. J. Zhao, M. Pumera, *J. Phys. Chem. C* **2014**, *118*, 5268 – 5274.
[31] M. Manjare, B. Yang, Y. P. Zhao, *J. Phys. Chem. C* **2013**, *117*, 4657 – 4665.
[32] G. S. Barker, B. Jefferson, S. J. Judd, *Chem. Eng. Sci.* **2002**, *57*, 565 – 573.
[33] W. Huang, M. Manjare, Y. Zhao, *J. Phys. Chem. C* **2013**, *117*, 21590 – 21596.
[34] M. Hashimoto, G. M. Whitesides, *Small* **2010**, *6*, 1051 – 1059.
[35] J. Simmchen, V. Magdanz, S. Sanchez, S. Chokmaviroj, D. Ruiz-Molina, A. Baeza, O. G. Schmidt, *RSC Adv.* **2014**, *4*, 20334 – 20340.

Manuscript received: March 25, 2019
Revised manuscript received: May 13, 2019
Accepted manuscript online: May 14, 2019
Version of record online: June 6, 2019